J. Phys.: Condens. Matter **23** (2011) 085001 (9pp) doi:10.1088/0953-8984/23/8/085001

Transverse and normal interfacial stiffness of solids with randomly rough surfaces

C Campañá[1], B N J Persson[2] and M H Müser[3]

[1] Department of Chemistry, University of Ottawa, Ottawa, ON, K1N 6N5, Canada
[2] IFF, FZ-Jülich, D-52425 Jülich, Germany
[3] Lehrstuhl für Materialsimulation, Universität des Saarlandes, D-66111 Saarbrücken, Germany

Received 29 September 2010
Published 3 February 2011
Online at stacks.iop.org/JPhysCM/23/085001

Abstract
Using a theoretical approach and computer simulations, we calculate the normal stiffness $K_\perp$ and the transverse stiffness $K_\parallel$ of the interface between two contacting isotropic solids with randomly rough surfaces and Poisson ratio ν. The theoretical predictions for $K_\perp$ agree well with the simulations. Moreover, the theoretical result for the ratio $K_\perp/K_\parallel$ is $(2-\nu)/(2-2\nu)$, as predicted by Mindlin for a single circular contact region. Finally, we compare the theory to experimental ultrasonic data.

(Some figures in this article are in colour only in the electronic version)

1. Introduction

Contact mechanics between solid surfaces is the basis for understanding many tribological processes [1–8] such as friction, adhesion, wear and sealing. The two most important properties in contact mechanics are the area of real contact and the interfacial separation between the solid surfaces. For non-adhesive contact and small squeezing pressure, the (projected) contact area has been found to depend linearly on the squeezing pressure [9–11].

When two elastic solids with rough surfaces are squeezed together, the solids will generally not make contact everywhere in the apparent contact area, but only at a distribution of asperity contact spots. The separation $u(\mathbf{x})$ between the surfaces will vary in a nearly random way with the lateral coordinates $\mathbf{x} = (x, y)$ in the apparent contact area. When the applied squeezing pressure increases, the average surface separation $u = \langle u(\mathbf{x})\rangle$ will decrease, but in most situations it is not possible to squeeze the solids into perfect contact corresponding to $u = 0$. One of us has recently developed a theory which predicts that, for randomly rough surfaces at low squeezing pressures, $p \sim \exp(-u/u_0)$, where the reference length u_0 depends on the nature of the surface roughness but is independent of p [2, 12]. From the relation $p = p(u)$ one can calculate the normal interfacial stiffness $K_\perp = -\mathrm{d}p/\mathrm{d}u = p/u_0$. In this paper we will show how one can obtain the transverse stiffness $K_\parallel$. We note that $K_\perp$ and $K_\parallel$ are very important for many applications, e.g. they determine the sound wave reflection from interfaces. Its measurement provides one of the most important clues in quantitative nondestructive evaluation on buried interfaces.

In a classical study, Mindlin [13] calculated the normal and transverse stiffness for the junction (with elliptic shape) formed by squeezing together two elastic bodies with quadratic surface profiles. For the special case of an elastic ball squeezed against a flat surface (giving a circular contact region) he found that the ratio between the normal and transverse stiffness is $K_\perp/K_\parallel = (2-\nu)/(2-2\nu)$, where ν is the Poisson ratio. Any theory which treats the contact regions between two elastic solids as (uncoupled) circular Hertzian contacts will give the same result for $K_\perp/K_\parallel$ as obtained by Mindlin. However, it is now known that neglecting the long-range elastic coupling between contact patches is a very severe approximation [11, 14–16]. Such theories neglect that, when an asperity is pushed downwards somewhere, the elastic deformation field extends a long distance away from the asperity, which will influence the contact involving other asperities further away [17]. The most prominent example is the Greenwood–Williamson (GW) model, in which rough surfaces are approximated by spherical bumps of equal radii. In the GW model the relation between the squeezing pressure and the (average) interfacial separation is Gaussian-like [10, 11, 15], $p \sim \exp(-bu^2)$ (where b is a constant determined by the nature of the roughness) rather than the (accurate) exponential relation [12] $p \sim \exp(-u/u_0)$. The GW theory makes the same error in the prediction of $K_\parallel$ as for $K_\perp$.

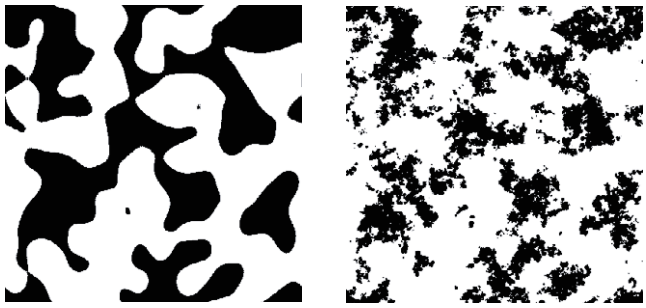

Figure 1. The contact region (black area) between two elastic solids observed at low (left) and high (right) magnification. For surfaces which have fractal-like roughness all the way down to the atomic length scale, the contact at the highest magnification (atomic resolution) typically consists of nanometer-sized clusters (right). The result in the picture was obtained using molecular dynamics (MD), but since there is no natural length scale in elastic continuum mechanics, it could also correspond to the contact between two macroscopic elastic solids. The contact stiffness mainly depends on the long-wavelength roughness and in general can be calculated accurately from the nature of the contact observed at low magnification (left). Adapted from [3].

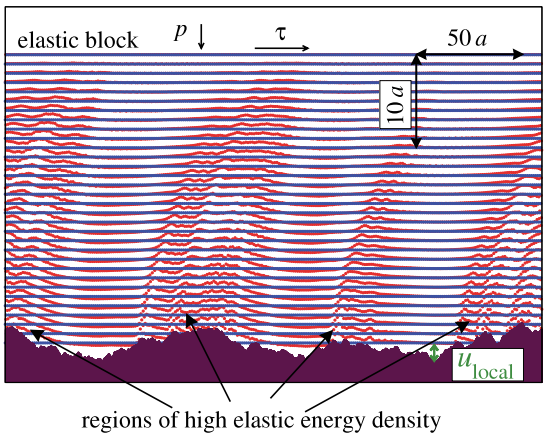

Figure 2. Snapshot of an elastic block squeezed against a rigid rough substrate as obtained in a small, two-dimensional, all-atom simulation. The separation between the average plane of the substrate and the average plane of the lower surface of the block is denoted by u, i.e. the average value of u_{local} shown in the figure. The elastic energy is stored in the block in the vicinity of the asperity contact regions. Normal and transverse directions have been represented by different scales, as indicated in the figure. The lattice constant a gives the spacing between two adjacent atoms in the elastic block.

Experimentally, $K_\perp/K_\parallel$ is approximately constant for contacts formed by rough solids [18]. This observation does not have to result from single-asperity mechanics, but may as well be due to the self-affine properties of most surface topographies, which result (for small load) in a pressure distribution that remains unchanged with load [9, 19–21] and produces fractal-like boundary lines [3, 22, 23], see figure 1. These boundaries differ from the circular (or elliptical) contact regions assumed in GW. Thus, both the normal and tangential stress in the contact regions will be much more complex than predicted by the Hertz and Mindlin theories. This is why one should try to avoid directly involving the nature of the contact regions when studying contact mechanics problems, such as the contact stiffness or the heat or electric contact resistance [24]. For all these reasons it remains unanswered as to why $K_\perp/K_\parallel$ is constant and what the value of this ratio is, when theories or simulations are used that properly reflect the elastic coupling between asperities. In the contact mechanics model of Persson [3, 9, 12, 19, 24, 25], which we use in the present study, long-range elastic coupling [16] is included.

Another important discovery is that, for elastic contact, the contact regions observed at atomic resolution may be just a few atoms wide, i.e. the diameter of the contact regions may be of the order of $\sim$1 nm [20, 26, 27]. The stress acting in such small contact regions may be very different from the stress acting in macroscopic contact regions. However, for macroscopic objects the contact stiffness is usually determined mainly by the nature of the contact observed at much lower magnification (i.e. larger length scales) and is therefore not sensitive to the atomistic nature of the contact, and can be accurately calculated using continuum mechanics. Finally, we note that for elastically hard solids the area of real (atomic) contact A may be a very small fraction of the nominal or apparent contact area A_0, even at high nominal squeezing pressures [7, 19].

The outline of this paper is as follows. In section 2.1 we briefly review the theory for $K_\perp$. In section 2.2 we derive an expression for the asperity-induced elastic energy due to an applied shear stress τ. In section 2.3 we derive an expression for $K_\perp/K_\parallel$ and an alternative derivation is presented in section 2.4. In section 3 we present numerical results for $K_\perp/K_\parallel$ and compare them to the theoretical prediction. In section 4 we review experimental results for $K_\perp/K_\parallel$ and compare it to the theory prediction. Section 5 contains the summary and conclusion.

2. Theory

2.1. Normal stiffness $K_\perp$

The theory presented in this paper for $K_\perp$ and $K_\parallel$ depends on the elastic energy (per unit area) $U_\perp$ and $U_\parallel$ stored in the asperity contact regions as a result of the applied squeezing pressure p and applied shear stress τ (see figure 2). The applied stresses result in a normal and transverse displacement of the (average) position of the bottom surface of the elastic block. We denote the (average) normal separation of the surfaces at the interface by u and the (average) transverse shift by v.

Consider first the frictionless contact between an elastic solid (elastic modulus E and Poisson ratio ν) with a flat surface and a rigid, randomly rough surface with the surface height profile $z = h(\mathbf{x})$. The separation between the average surface plane of the block and the average surface plane of the substrate (see figure 2) is denoted by u with $u \geqslant 0$. When the applied squeezing force p increases, the separation between the surfaces at the interface will decrease and we can consider $p = p(u)$ as a function of u. The elastic energy $U_\perp(u)$ stored (per unit surface area) in the substrate asperity–elastic block contact regions must be equal to the work done by the external pressure p in displacing the lower surface of the block towards

the substrate. Thus

$$p(u) = -\frac{\mathrm{d}U_\perp}{\mathrm{d}u}. \tag{1}$$

For elastic solids (1) is exact [12, 25].

Theory shows that, with increasing p, existing contact areas grow and new contact areas form in such a way that, in the thermodynamic limit (infinitely large system), the interfacial stress distribution, and also the size distribution of contact spots, are independent of the squeezing pressure as long as these distributions are normalized to the real contact area A [19]. From this it follows immediately that A varies linearly with the squeezing force pA_0. Thus, the just-mentioned distribution functions will scale linearly with p when they are normalized to A_0 (the apparent contact area) rather than to A. The same linear scaling will be found for any quantity that derives from the stress distributions within the vicinity of true asperity contact, such as the elastic energy $U_\perp$ stored there. (Note that the elastic energy density is more localized than stress or strain fields are, because it is proportional to their squares, see also figure 2.) Thus at small loads, $U_\perp(u) = u_0 p(u)$, where u_0 must be of dimension length. Equation (1) then takes the form

$$p(u) = -u_0 \frac{\mathrm{d}p}{\mathrm{d}u}, \tag{2}$$

and the normal stiffness becomes

$$K_\perp = -\frac{\mathrm{d}p}{\mathrm{d}u} = \frac{p}{u_0}, \tag{3}$$

i.e. the stiffness is proportional to the nominal squeezing pressure p. Note also that from equation (2) we get

$$p(u) \sim \mathrm{e}^{-u/u_0}. \tag{4}$$

Further analysis, see [12], shows that u_0 is of the order of the root-mean-square roughness amplitude, but (as assumed above) independent of p.

In [28] (see also [29]) we presented experimental results to test the theory predictions. We studied the squeezing of a rubber block against an asphalt road surface and found good agreement between the theory (equation (4)) and the experiments.

2.2. Elastic energies $U_\perp$ and $U_\parallel$

Consider the contact between two elastic solids with rough surfaces. We can write the elastic energy (per unit area) induced by the normal stress and stored in the vicinity of the asperity contact regions as

$$U_\perp = \frac{1}{2A_0}\int \mathrm{d}^2x\, \langle \sigma_z(\mathbf{x}) u_z(\mathbf{x})\rangle, \tag{5}$$

where A_0 is the nominal contact area, and where $u_z(\mathbf{x})$ and $\sigma_z(\mathbf{x})$ are the normal displacement and the normal stress, respectively. We write

$$\sigma_z(\mathbf{x}) = \int \mathrm{d}^2q\, \sigma_z(\mathbf{q}) \mathrm{e}^{\mathrm{i}\mathbf{q}\cdot\mathbf{x}}, \tag{6}$$

and similar for $u_z(\mathbf{x})$. Substituting this in (5) gives

$$U_\perp = \frac{(2\pi)^2}{2A_0}\int \mathrm{d}^2q\, \langle \sigma_z(\mathbf{q}) u_z(-\mathbf{q})\rangle, \tag{7}$$

or using (see the appendix)

$$u_z(\mathbf{q}) = M_{zz}(\mathbf{q})\sigma_z(\mathbf{q}) = (\rho c_\mathrm{T}^2 q)^{-1}(1-\nu)\sigma_z(\mathbf{q}), \tag{8}$$

we get

$$U_\perp = \frac{(2\pi)^2}{2A_0}\frac{1-\nu}{\rho c_\mathrm{T}^2}\int \mathrm{d}^2q\, q^{-1}\langle |\sigma_z(\mathbf{q})|^2\rangle. \tag{9}$$

It is interesting to note that in most cases the largest contribution to the elastic energy arises from the long-wavelength roughness components. This is clear if we note that for self-affine fractal surfaces characterized by the Hurst exponent H (or the fractal dimension $D_\mathrm{f} = 3 - H$) we have the (probably exact) scaling relation [14, 16] $\langle |\sigma_z(\mathbf{q})|^2\rangle \sim q^{-(1+H)}$. Using this relation in (9) gives

$$U_\perp \sim \int_{q_0}^{q_1} \mathrm{d}q\, q^{-(1+H)} \sim q_0^{-H} - q_1^{-H}.$$

Since $0 < H < 1$ (and typically $H \approx 0.8$) the elastic energy is dominated by the most-long-wavelength roughness components (say, by the last decade of roughness wavelength, corresponding to the range of wavevectors $q_0 < q < 10q_0$). Since the stiffness $K_\perp$ is determined by the elastic energy (see section 2.1) the same conclusion holds for the stiffness. The same conclusion can be derived by studying how different surface roughness components contribute to the length u_0 (see [24] for such an analysis).

Let us now apply a shear stress to the block with the force vector pointing along the x axis. This will induce an elastic energy (per unit area) stored in the asperity contact regions and given by

$$U_\parallel = \frac{1}{2A_0}\int \mathrm{d}^2x\, \langle \sigma_x(\mathbf{x}) u_x(\mathbf{x})\rangle. \tag{10}$$

We have (see the appendix)

$$u_x(\mathbf{q}) = M_{xx}(\mathbf{q})\sigma_x(\mathbf{q}) = (\rho c_\mathrm{T}^2 q)^{-1}[1-\nu+\nu\cos^2\phi]\sigma_x(\mathbf{q}), \tag{11}$$

where ϕ is the angle between $\hat{x}$ and $\mathbf{e} = \hat{z}\times\hat{q}$. Substituting this in (10) gives

$$U_\parallel = \frac{(2\pi)^2}{2A_0}\frac{1}{\rho c_\mathrm{T}^2}\int \mathrm{d}^2q\, q^{-1}[1-\nu+\nu\cos^2\phi]\langle |\sigma_x(\mathbf{q})|^2\rangle. \tag{12}$$

For a single circular contact region (Mindlin case), the stress in the contact region depends only on the distance r from the center of the contact region, so in this case $\sigma_x(\mathbf{q})$ depends only on $q = |\mathbf{q}|$. We expect this to hold as a good approximation in the present case and we will assume that $\langle |\sigma_x(\mathbf{q})|^2\rangle$ depends only on q. In this case we can replace the term $\cos^2\phi$ in (10) by its angular average $1/2$. This gives

$$U_\parallel = \frac{(2\pi)^2}{2A_0}\frac{2-\nu}{2\rho c_\mathrm{T}^2}\int \mathrm{d}^2q\, q^{-1}\langle |\sigma_x(\mathbf{q})|^2\rangle. \tag{13}$$

We expect $\langle|\sigma_x(\mathbf{q})|^2\rangle \sim q^{-(1+H)}$ to obey the same scaling as for the perpendicular stress. Thus $U_\parallel$ and hence $K_\parallel$ will, just like for $U_\perp$ and $K_\perp$, be dominated by the most-long-wavelength surface roughness components, i.e. short-wavelength (e.g. nanometer) roughness is irrelevant. This also implies that plastic yield and adhesion occurring in the contact regions observed at very high magnification (i.e. at short length scale) may have a negligible influence on the contact stiffness in most cases. A similar conclusion was drawn in [24] for the heat and electric contact resistance.

2.3. Transverse stiffness $K_\parallel$

Consider (11) and assume we can replace $\cos^2\phi$ with its angular average 1/2. We get

$$u_x(\mathbf{q}) = (2\rho c_T^2 q)^{-1}(2-\nu)\sigma_x(\mathbf{q}), \tag{14}$$

which has the same form as (8) except for a numerical prefactor. Thus one may be tempted to infer that the displacement and stress fields of the two contact mechanics problems are proportional to each other. However, this is not the case since the two problems involves different boundary conditions: the parallel displacement $u_x(\mathbf{x})$ is continuous in the contact regions (since we assume no-slip boundary condition) while $u_z(\mathbf{x})$ in the contact regions depend on the gap function $h(\mathbf{x})$. In particular, if the substrate is rigid, then $u_x(\mathbf{x}) = 0$ and $u_z(\mathbf{x}) = h(\mathbf{x})$ in the asperity contact regions. That the solutions of the two problems differ is, of course, well known for the Mindlin problem of a single circular contact region, where $\sigma_z \sim [1-(r/r_0)^2]^{1/2}$ while $\sigma_x \sim [1-(r/r_0)^2]^{-1/2}$. However, as we now show, one can remove this difference in the boundary conditions by reformulating the problem above by using a simple observation first applied by Barber [30] (but here we follow the presentation given in [24]) to the related problem of the electric (or thermal) contact resistance between elastic solids with randomly rough surfaces.

Note that u_z and σ_z depend on the normal stress or pressure p applied to the upper surface of the block. Alternatively, since the average separation u between the surfaces at the interface decreases monotonically with increasing p we can consider u_z and σ_z to depend parametrically on u. Let us take the derivative of (8) with respect to u. Denoting $\mathrm{d}u_z/\mathrm{d}u = u_z'$ and similar for σ_z gives

$$u_z'(\mathbf{q}) = (\rho c_T^2 q)^{-1}(1-\nu)\sigma_z'(\mathbf{q}), \tag{15}$$

with the boundary conditions that $\sigma_z'(\mathbf{x})$ vanish in the non-contact region while $u_z'(\mathbf{x})$ vanish in the contact regions (since $h(\mathbf{x})$ is *independent of* u). In addition, the condition

$$\frac{1}{A_0}\int \mathrm{d}^2x\, \sigma_z(\mathbf{x}) = p,$$

takes the form

$$\frac{1}{A_0}\int \mathrm{d}^2x\, \sigma_z'(\mathbf{x}) = p'.$$

If we denote $\psi_z = \sigma_z'/p'$ we can write

$$\frac{1}{A_0}\int \mathrm{d}^2x\, \psi_z(\mathbf{x}) = 1,$$

and (15) takes the form

$$\phi_z(\mathbf{q}) = q^{-1}\psi_z(\mathbf{q}), \tag{16}$$

where

$$\phi_z = \rho c_T^2(1-\nu)^{-1}u_z'/p'. \tag{17}$$

Note that u_x and σ_x depend on the tangential stress τ applied to the upper surface of the block and obey equation (14). The relevant boundary conditions are that $\sigma_x(\mathbf{x})$ vanishes in the non-contact region while $u_x(\mathbf{x})$ vanishes in the contact regions (since $u_x(\mathbf{x}) = 0$ in the contact area; no-slip boundary condition). In addition we must have

$$\frac{1}{A_0}\int \mathrm{d}^2x\, \sigma_x(\mathbf{x}) = \tau.$$

If we denote $\psi_x = \sigma_x/\tau$ we can write

$$\frac{1}{A_0}\int \mathrm{d}^2x\, \psi_x(\mathbf{x}) = 1,$$

and (14) takes the form

$$\phi_x(\mathbf{q}) = q^{-1}\psi_x(\mathbf{q}), \tag{18}$$

where

$$\phi_x = 2\rho c_T^2(2-\nu)^{-1}u_x/\tau. \tag{19}$$

Note that the systems of equations for (ϕ_z, ψ_z) and (ϕ_x, ψ_x) are identical and therefore $\phi_z = \phi_x$ and $\psi_z = \psi_x$. Using that $\phi_z = \phi_x$, from (17) and (19) we get

$$u_z'(\mathbf{x}) = \frac{2(1-\nu)}{2-\nu}\frac{p'}{\tau}u_x(\mathbf{x}). \tag{20}$$

Next we note that

$$\int \mathrm{d}^2x\, u_z'(\mathbf{x}) = \frac{\mathrm{d}}{\mathrm{d}u}\int \mathrm{d}^2x\, u_z(\mathbf{x}) = \frac{\mathrm{d}}{\mathrm{d}u}A_0u = A_0,$$

while

$$\int \mathrm{d}^2x\, u_x(\mathbf{x}) = A_0v.$$

Thus, integrating (20) over $\mathbf{x}$ gives

$$A_0 = \frac{2(1-\nu)}{2-\nu}\frac{p'}{\tau}A_0v, \tag{21}$$

or using that $K_\parallel v = \tau$ and $p' = K_\perp$ we get

$$\frac{K_\perp}{K_\parallel} = \frac{2-\nu}{2-2\nu}, \tag{22}$$

which is the same as the Mindlin result for a single circular contact region.

2.4. Alternative derivation of $K_\parallel$

In section 2.2 we derived the following expression for the elastic energy (per unit area) induced by the normal stress and stored in the vicinity of the asperity contact regions:

$$U_\perp = \frac{(2\pi)^2}{2A_0}\frac{1-\nu}{\rho c_T^2}\int \mathrm{d}^2q\, q^{-1}\langle|\sigma_z(\mathbf{q})|^2\rangle. \tag{23}$$

Similarly, the elastic energy induced by a parallel stress

$$U_\parallel \approx \frac{(2\pi)^2}{2A_0}\frac{2-\nu}{2\rho c_{\mathrm{T}}^2}\int \mathrm{d}^2q\, q^{-1}\langle|\sigma_x(\mathbf{q})|^2\rangle. \tag{24}$$

Note that $\sigma_z(\mathbf{q})$ and $\sigma_x(\mathbf{q})$ depend on the spatial variation of $\sigma_z(\mathbf{x})$ and $\sigma_x(\mathbf{x})$, respectively. There are two contributions to the spatial dependence of the stress, namely one derived from the variation of the stress within a contact region, which of course differs for $\sigma_z(\mathbf{x})$ and $\sigma_x(\mathbf{x})$, and one derived from the fact that the stress is non-vanishing only in the area of real contact, and this spatial dependence is the same for $\sigma_z(\mathbf{x})$ and $\sigma_x(\mathbf{x})$. If the latter contribution would dominate in the integrals (23) and (24) one would expect

$$\int \mathrm{d}^2q\, q^{-1}\frac{\langle|\sigma_x(\mathbf{q})|^2\rangle}{\tau^2} \approx \int \mathrm{d}^2q\, q^{-1}\frac{\langle|\sigma_z(\mathbf{q})|^2\rangle}{p^2} \tag{25}$$

which effectively would mean that

$$\sigma_x(\mathbf{x})/\tau \approx \sigma_z(\mathbf{x})/p, \tag{26}$$

where τ is the average shear stress and p the average normal stress[4]. However, the correct result (for small load, where the area of real contact is proportional to the load) is

$$\int \mathrm{d}^2q\, q^{-1}\frac{\langle|\sigma_x(\mathbf{q})|^2\rangle}{\tau^2} \approx \frac{1}{2}\int \mathrm{d}^2q\, q^{-1}\frac{\langle|\sigma_z(\mathbf{q})|^2\rangle}{p^2}. \tag{27}$$

Using (24) and (27) we get

$$U_\parallel = \frac{(2\pi)^2}{2A_0}\frac{2-\nu}{4\rho c_{\mathrm{T}}^2}\left(\frac{\tau}{p}\right)^2\int \mathrm{d}^2q\, q^{-1}\langle|\sigma_z(\mathbf{q})|^2\rangle. \tag{28}$$

Comparing this to (23) gives

$$U_\parallel = \frac{2-\nu}{4(1-\nu)}\left(\frac{\tau}{p}\right)^2 U_\perp. \tag{29}$$

We can also write

$$U_\parallel = \frac{1}{2}K_\parallel v^2 = \frac{1}{2}\frac{\tau^2}{K_\parallel}. \tag{30}$$

Using (29) and (30) and that $p/u_0 = K_\perp$ and $U_\perp = u_0 p$ we get

$$\frac{K_\perp}{K_\parallel} = \frac{2-\nu}{2-2\nu}. \tag{31}$$

3. Simulations

3.1. Method

To assert the validity of the theory presented in this work, numerical simulations were performed using the Green's function molecular dynamics (GFMD) technique [31]. In GFMD, all the degrees of freedom related to the atoms that do not belong to the bottom surface of the elastic block are integrated out. Such integration of degrees of freedom yields a two-dimensional elastic layer with renormalized atomic forces that is equivalent to the original three-dimensional elastic block. By 'equivalent' we imply that the GFMD layer deforms identically to the bottom surface of the original three-dimensional elastic block under the action of an external squeezing pressure. Thus, lowering the dimensionality of the problem via GFMD allows one to simulate larger contact interfaces which represent better the continuum limit.

The interaction of the manifold atoms with the walls is modeled via a hard-wall potential. Whenever the atoms have violated the constraint that they have to remain above the substrate at the end of a molecular dynamics time step, they are artificially moved right on top of the substrate and their velocity is zeroed. This is done until convergence is achieved. The force between manifold atom and wall is then determined indirectly by calculating the force within the manifold. These two forces must have the same magnitude but opposite sign in mechanical equilibrium.

In the GFMD simulations presented here, we created randomly rough surfaces using a Fourier filtering algorithm [14]. The surfaces satisfied the small-slope approximation with an rms roughness slope of ≈0.032. Different values of the Hurst exponents were taken into account, i.e. $H = 0.3, 0.5$ and 0.8. The system size was kept fixed at a default size $N = 2048 \times 2048$ and a hard cutoff at a default value of $q_{\mathrm{c}} = 64$ (in units of $2\pi/\mathcal{L}$, where $\mathcal{L}$ is the linear dimension of the simulation cell) was imposed in order to reach the continuum limit reasonably well (the shortest wavelength divided by the lattice spacing equals 32). We did not explore roughness down to the smallest scales, because our goal was to test the validity of the solutions of a continuum theory rather than to ascertain potential effects due to atomic-scale roughness. A representative plot showing one of our surface topographies and its height–height correlation function is portrayed in figure 3.

In order to ensure that our GFMD methodology is properly implemented for the particular problem concerning us here, we verified that our GFMD simulations could reproduce the analytical prediction of Mindlin for a single spherical Hertzian tip [13]. The elastic manifold employed in such a test had Young modulus $E = 2.5$ and Poisson ratio $\nu = 1/4$ which gives a Mindlin stiffness ratio $K_\perp/K_\parallel = (2-\nu)/(2-2\nu) = 7/6$. As expected, the previous analytical prediction was properly reproduced by the numerical calculations. For system sizes of $N = 256 \times 256$, 512×512 and 1024×1024 we obtained $K_\perp/K_\parallel = 1.1365$, 1.1421 and 1.1512, respectively, all in good agreement with the $K_\perp/K_\parallel = 7/6 \approx 1.1666$ value stated by the theory. The difference between the computed stiffness ratio and the exact one seems to disappear according to the power law $N^{-1/4}$. We will use this scaling later in our simulations of rough solids. Of course, there the prefactor for the corrections will be distinctly larger, because each individual contact patch will be much less resolved than in the Hertzian test case.

[4] In [24] one of us used a very similar approach to the contact heat transfer problem (which has great mathematical similarities to the contact stiffness problem). In appendix A in [24] it was argued that an equation similar to (25) holds, with σ_x/τ replaced by J_z/J_0, where J_z is the heat current at the interface and J_0 the average heat current. However, the correct relation will have an additional factor of 1/2 as in (27) and the expression for the heat transfer coefficient α (given by (26b) in [24]) should have an additional factor of 2.

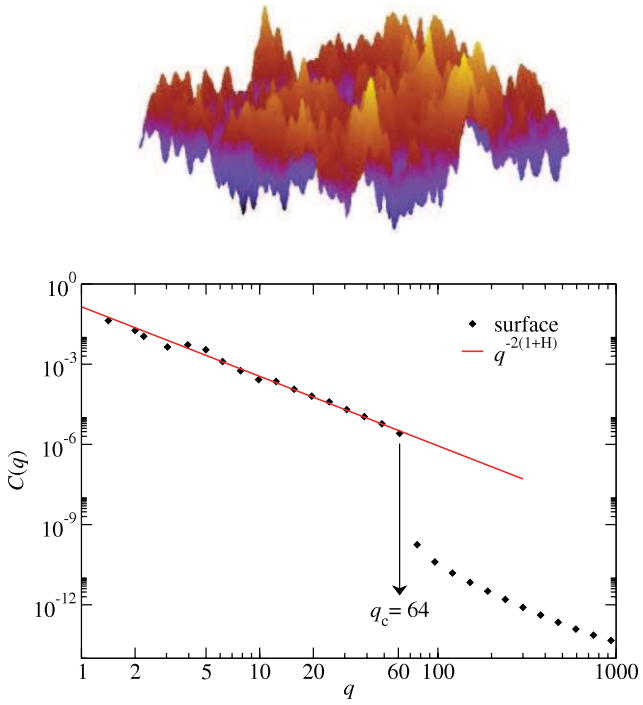

Figure 3. Graphical representation of a rough topography with Hurst exponent $H = 0.3$ and its corresponding height–height correlation function $C(q) = \langle |h(\mathbf{q})|^2 \rangle$ in Fourier space. The surface topography was created using a Fourier filtering technique and a hard cutoff $q_c = 64$ was imposed on it in Fourier space (in units of $2\pi/\mathcal{L}$, where $\mathcal{L}$ is the linear dimension of the simulation cell). The continuous line represents the ideal algebraic scaling expected for the height–height correlation function of such a surface.

Next, a second (cross-validation) test was done and compared to previous molecular dynamics simulations that had been performed by some of us [32, 33] using the smart block method on smaller surfaces and at a fixed value ($H = 0.8$) of the Hurst exponent. For this comparison we replaced the Green's function for elastically isotropic solids with those for cubic systems that would have been relevant for the older simulations. In these simulations we (re-)validated the exponential functional form relating squeezing pressure and average interfacial separation in rough contacts, derived in [12]. All simulations shown in the following had been based on an isotropic Green's function, because the theory has been specifically developed for isotropic solids.

3.2. Results

In order to calculate the relation $p(u)$ between the pressure p and the interfacial separation u, we need an accurate expression for the elastic energy stored in the asperity contact region. The elastic energy $U_\perp = U_{\rm el}$ is written as [16, 19, 34]

$$U_{\rm el} = \frac{E A_0}{4(1-\nu^2)} \int {\rm d}^2 q \, q C(q) W(q). \tag{32}$$

For complete contact $W(q) = 1$ rendering an exact result for the expression of the energy above. In [34] it was argued that $W(q) = P(q) = A(\zeta)/A_0$ is the relative contact area when the interface is studied at the magnification $\zeta = q/q_0$. The qualitative explanation is that the solids will mainly deform in the regions where they make contact, thus most of the elastic energy will arise from the contact regions. Using $W(q) = P(q)$ assumes that the energy (per unit area) in the asperity contact regions is just the average elastic energy (per unit area) if complete contact would occur. This does not take into account that the regions where no contact occurs are those regions where most elastic energy (per unit area) would be stored if complete contact would occur. Hence we expect smaller stored elastic energy (per unit area) in the asperity contact regions than obtained using $W(q) = P(q)$. In [16, 25] we found that using

$$W(q) = P(q)[\gamma + (1-\gamma)P^2(q)], \tag{33}$$

with $\gamma \approx 0.4$ gives good agreement between theory and MD simulations for $H = 0.8$. Note that for complete contact $P(q) = 1$ and hence $W(q) = 1$, which reduces to the exact result for the elastic energy in the limit of complete contact. In the limit of small contact, $P(q) \ll 1$, then $W(q) \approx \gamma P(q)$ and with $\gamma \approx 0.4$ this result in an elastic energy which is a factor of 0.4 smaller than would result if the elastic energy (per unit area) stored in the contact regions would be just the average elastic energy (per unit area) for complete contact.

Using the elastic energy expressions given by (32) and (33), for small squeezing pressures, results in a relation $p \sim \exp(-u/u_0)$, where $u_0 \sim \gamma$. The area of real contact for small load (where $A \sim p$) also turns out to be a function of γ and in [16] we have shown that it scales as $\gamma^{-1/2}$. This dependence of A on γ improves the agreement between theory and numerically accurate simulations, which typically gave a contact area somewhat larger than predicted by theory with $\gamma = 1$. Thus for $H = 0.8$ the improved elastic energy given by (32) and (33) gives good agreement between theory and computer simulations both for the contact area and the interfacial separation. Here we show that using $\gamma = 0.45$ gives good agreement between theory and computer simulations also for $H = 0.3$ and 0.5.

Comparison between the GFMD data and the theoretical predictions is displayed in figure 4. As shown, the match between the simulated and predicted behavior is very good. Theory and simulations of rough contacts agreed in the functional form that describes the applied pressure p as a function of the average separation u over a wide range of pressure values and roughness exponents. Recently, a value of $\gamma = 0.48$ has been independently reported by Akarapu *et al* [37] after analyzing a variety of rough contacts with roughness down to the atomic scale, variable Poisson ratio and $H = 0.5$ and 0.8.

Similarly, the theoretical predictions and the numerical outcome conveyed in describing the dependence of the fractional contact area A/A_0 as a function of the external pressure. Support for the latter claim is provided in figure 5. The results of the aforementioned calculations served to strengthen our confidence in the correct application of GFMD when measuring normal and transverse stiffness ratios in rough contacts.

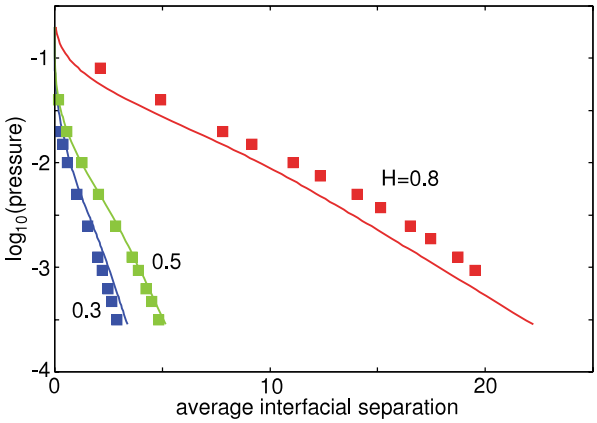

Figure 4. Relation between applied squeezing pressure p and average interfacial separation u: comparison between the GFMD simulation data (for $N = 2048 \times 2048$ and $q_c = 64$) and analytical predictions for surfaces with distinct values of the Hurst exponent.

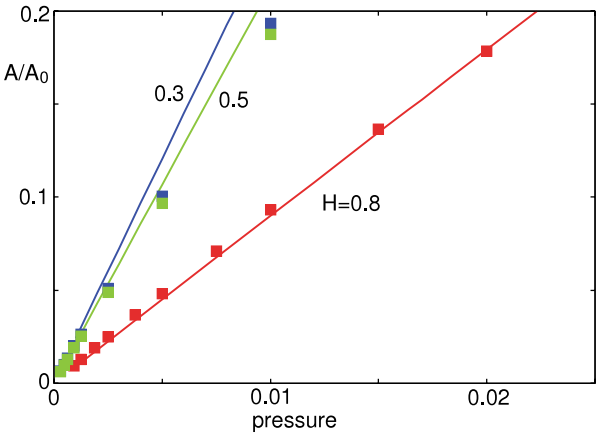

Figure 5. Relative contact area A/A_0 as a function of the applied pressure p for the surfaces corresponding to the results presented in figure 4.

For the calculation of the $K_\perp/K_\parallel$ ratio in rough contacts we performed simulations in which the GFMD layer resolution, the surface cutoff, the random seed, the pressure and the rms slope of the surfaces were varied. However, the elastic properties of the GFMD layer remained unaltered. Furthermore, two distinct ways of estimating $K_\perp$ were considered. In the first one, $K_\perp$ was ascertained from the analytical slope of the pressure versus average interfacial separation plots shown in figure 4. In the second approach $K_\perp$ was computed by taking the finite differences ratio $\Delta p/\Delta u$ in the limit of small Δp at fixed contact area. We did not find noticeable differences between using either one of the two approaches. Our numerical findings followed closely the analytical predictions of the theory introduced in the past sections. Results are shown in figure 6. One can see that the numerical estimates seem to be somewhat larger than the Mindlin ratio, however, only by ∼12%. These calculations are plagued with large numerical scatter so that a precise determination of the $K_\perp/K_\parallel$ ratio is rather difficult.

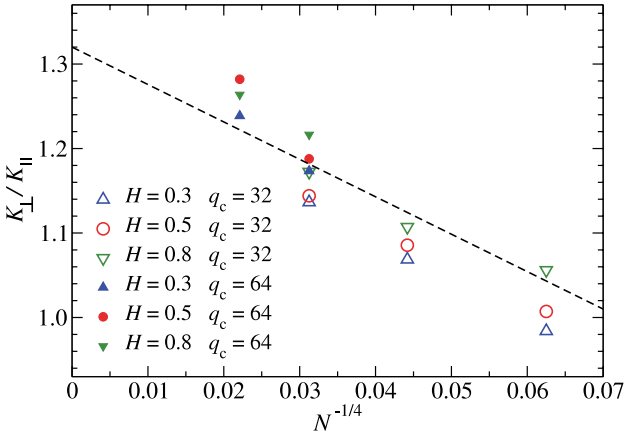

Figure 6. Stiffness ratio $K_\perp/K_\parallel$ as a function of $N^{-1/4}$, where N is the linear system size for different cutoff wavenumbers q_c and Hurst roughness exponents H. Errors are about 0.1 for each measurement.

4. Discussion of ultrasonic data

The interfacial stiffness can be measured using ultrasonic wave interaction. In these experiments ultrasonic sound waves are sent onto the interface under study. From the measured shear and longitudinal reflection and transmission coefficients one can deduce $K_\perp$ and $K_\parallel$, assuming that the wavelength λ of the sound waves is much larger than the size and typical distance between the asperity contact regions. (More precisely, λ must be large compared to λ_0, where $q_0 = 2\pi/\lambda_0$ is the roll-off wavevector of the surface roughness power spectrum.) The reason the reflection factor depends on $K_\perp$ and $K_\parallel$ is that these quantities enter in the boundary conditions necessary in solving the sound wave propagation at the interface. These boundary conditions consist of the continuity of the tangential stress σ_{zx} and the normal stress σ_{zz}, while the displacement is discontinuous and determined by

$$\sigma_{zz} = K_\perp[u_z(0^+) - u_z(0^-)],$$

$$\sigma_{zx} = K_\parallel[u_x(0^+) - u_x(0^-)],$$

where $u(0^+)$ and $u(0^-)$ are the displacement just above and just below the contacting interface, respectively.

A large number of ultrasonic measurements of $K_\perp$ and $K_\parallel$ have been presented in the literature. For example, Baltazar *et al* [35] studied the stiffness of the interface between two aluminum blocks with randomly rough surfaces prepared by sandpaper grinding and by sandblasting. The root-mean-square roughness was in the range 0.2–0.7 μm. The ratio $K_\parallel/K_\perp$ for low nominal contact pressure was 0.42 ± 0.03, which should be compared with the theory prediction (equation (17) with $\nu = 0.33$): 0.80. A summary of some earlier ultrasonic measurements of $K_\parallel/K_\perp$ was presented by Nagy [36] which we reproduce below.

Wooldridge, steel surfaces (root-mean-square roughness 0.2 μm):

$$K_\parallel/K_\perp(\text{exp}) = 0.38 \pm 0.1, \qquad K_\parallel/K_\perp(\text{theory}) = 0.84.$$

Pyrak-Nolte *et al*, fractured granite surfaces:

$$0.40(\text{exp}), \qquad 0.84(\text{theory}).$$

Yoshioka *et al*, granite surfaces (2–10 μm):

$$0.32 \pm 0.05(\text{exp}), \qquad 0.84(\text{theory}).$$

Pyrak-Nolte *et al*, steel surfaces:

$$0.26(\text{exp}), \qquad 0.84(\text{theory}).$$

Nagy *et al*, aluminum surfaces (0.5 μm):

$$0.38(\text{exp}), \qquad 0.80(\text{theory}).$$

Hsu *et al*, poly(methyl methacrylate):

$$0.45 \pm 0.1(\text{exp}), \qquad 0.80(\text{theory}).$$

It is clear from these data that, on average, the experimental results for $K_\parallel/K_\perp$ are about half of what is predicted by theory.

5. Summary and conclusion

In this paper we have extended Persson's contact mechanics theory to the calculation of the lateral stiffness $K_\parallel$ of a mechanical interface formed by two solids with rough surfaces. This was done by assuming that no slip occurs at the true contact points under a small external shear stress. The problem of finding the dependence between lateral displacement and shear stress was then mapped onto a similar dependence for normal displacement and normal stress, which, however, required a reformulation of the boundary conditions. The resulting quotient of $K_\parallel$ and the normal stiffness $K_\perp$ turned out to be $K_\parallel/K_\perp = (2-2\nu)/(2-\nu)$, where ν is the Poisson ratio. This result is identical to that found by Mindlin for spherical contacts. As the theory for $K_\perp$ had already been developed previously and shown to exhibit the correct linear dependence on load, and exponential dependence on the interfacial separation, the present paper implicitly contains a derivation of how $K_\parallel$ depends on these variables as well. The presented theory gives information about which length scales are most important for the determination of the contact stiffness, and can be generalized in various ways, e.g. to include adhesion [32].

The theoretical results have been tested with large-scale molecular dynamics simulations. First, we have shown that the theory for the load–displacement relation works well for different Hurst roughness exponents, complementing already existing experimental and numerical evidence. The present confirmation of the theory on $K_\perp$ has the advantage that our elastic solid was isotropic (as opposed to cubic in previous simulations), and that the assumptions made in the model, such as hard-wall interactions, no adhesion, exactly known height profiles, linear elasticity, etc, are better realized in the simulations than in experiment. Next, we computed the stiffness ratio. This calculation turned out to be plagued by large numerical scatter and size effects. However, most results were close to the theoretical predictions. Despite the remaining uncertainties about the precise value, we feel confident to rule out that the exact solution of the model would produce the relatively large stiffness ratios observed in ultrasonic measurements that had been conducted in the context of nondestructive evaluation on buried interfaces, and turned out to be twice the Mindlin result for spherical contacts. This may result from small (lateral) slip in the contact regions (as already suggested in [37]), which would effectively reduce $K_\parallel$ or may be caused by other effects such as adhesion or plastic yielding, which was not included in the theory presented above.

Acknowledgments

This work, as part of the European Science Foundation EUROCORES Program FANAS, was supported from funds by the DFG and the EC Sixth Framework Program, under contract N ERAS-CT-2003-980409. Conversations with Mark Robbins are gratefully acknowledged.

Appendix

Using the theory of elasticity (assuming an isotropic elastic medium for simplicity), one can calculate the displacement field u_i on the surface $z = 0$ in response to the surface stress distributions $\sigma_i = \sigma_{3i}$. Let us define the Fourier transform

$$u_i(\mathbf{q},\omega) = \frac{1}{(2\pi)^3}\int \mathrm{d}^2x\,\mathrm{d}t\; u_i(\mathbf{x},t)\mathrm{e}^{-\mathrm{i}(\mathbf{q}\cdot\mathbf{x}-\omega t)},$$

and similar for $\sigma_i(\mathbf{q},\omega)$. Here $\mathbf{x} = (x, y)$ and $\mathbf{q} = (q_x, q_y)$ are two-dimensional vectors. In [9] we showed that

$$u_i(\mathbf{q},\omega) = M_{ij}(\mathbf{q},\omega)\sigma_j(\mathbf{q},\omega),$$

or, in matrix form,

$$\mathbf{u}(\mathbf{q},\omega) = M(\mathbf{q},\omega)\boldsymbol{\sigma}(\mathbf{q},\omega),$$

where the matrix (see [9]):

$$M = -\frac{\mathrm{i}}{\rho c_\mathrm{T}^2}\left(\frac{1}{S(q,\omega)}\left[Q(k,\omega)(\hat{z}\mathbf{q}-\mathbf{q}\hat{z}) + \left(\frac{\omega}{c_\mathrm{T}}\right)^2\left(p_\mathrm{L}\hat{z}\hat{z}+p_\mathrm{T}\hat{q}\hat{q}\right)\right] + \frac{1}{p_\mathrm{T}}\mathbf{ee}\right), \tag{A.1}$$

where $\hat{q} = \mathbf{q}/q$, $\mathbf{e} = \hat{z}\times\hat{q}$ and where

$$S = \left(\frac{\omega^2}{c_\mathrm{T}^2} - 2q^2\right)^2 + 4q^2 p_\mathrm{T} p_\mathrm{L},$$

$$Q = 2q^2 - \omega^2/c_\mathrm{T}^2 + 2p_\mathrm{T}p_\mathrm{L},$$

$$p_\mathrm{T} = \pm\left(\frac{\omega^2}{c_\mathrm{T}^2} \pm \mathrm{i}\epsilon - q^2\right)^{1/2},$$

$$p_\mathrm{L} = \pm\left(\frac{\omega^2}{c_\mathrm{L}^2} \pm \mathrm{i}\epsilon - q^2\right)^{1/2},$$

where the $+$ and $-$ signs refer to $\omega > 0$ and $\omega < 0$, respectively, and where ϵ is an infinitesimal positive number.

In the equations above, ρ, c_T and c_L are the mass density, and the transverse and longitudinal sound velocities of the solid, respectively. Note that c_T and c_L are complex frequency-dependent quantities given by

$$c_T^2 = \frac{E}{2\rho(1+\nu)},$$
$$c_L^2 = \frac{E(1-\nu)}{\rho(1+\nu)(1-2\nu)},$$

where $E(\omega)$ is the complex elastic modulus and $\nu(\omega)$ is the Poisson ratio.

Here we are interested in low frequencies ω. As $\omega \to 0$ equation (A.1) reduces to

$$M = -\frac{1}{2\rho c_T^2 q}\left[-\mathrm{i}(1-2\nu)(\hat{z}\hat{q} - \hat{q}\hat{z}) + 2(1-\nu) + 2\nu\mathbf{ee}\right].$$

It is interesting to note that, for an incompressible material, $\nu = 0.5$, there is no coupling between the transverse and normal directions, e.g. a normal stress gives a purely normal displacement and a transverse stress a purely transverse displacement. Note that

$$M_{zz} = -(\rho c_T^2 q)^{-1}(1-\nu),$$

and

$$M_{xx} = -(\rho c_T^2 q)^{-1}[1 - \nu + \nu\cos^2\phi],$$

where ϕ is the angle between $\hat{x}$ and $\mathbf{e}$.

References

[1] Persson B N J, Albohr O, Tartaglino U, Volokitin A I and Tosatti E 2005 *J. Phys.: Condens. Matter* **17** R1
[2] Benz M, Rosenberg K J, Kramer E J and Israelachvili J N 2006 *J. Phys. Chem.* B **110** 11884
[3] Persson B N J and Yang C 2008 *J. Phys.: Condens. Matter* **20** 315011
[4] Persson B N J 2008 *J. Phys.: Condens. Matter* **20** 315007
[5] Bowden F P and Tabor D 1956 *Friction and Lubrication of Solids* (New York: Wiley)
[6] Johnson K L 1985 *Contact Mechanics* (Cambridge: Cambridge University Press)
[7] Persson B N J 2000 *Sliding Friction: Physical Principles and Applications* 2nd edn (Heidelberg: Springer)
[8] Israelachvili J N 1995 *Intermolecular and Surface Forces* (London: Academic)
[9] Persson B N J 2001 *J. Chem. Phys.* **115** 3840
[10] Greenwood J A and Williamson J B P 1966 *Proc. R. Soc.* A **295** 300
[11] Carbone G and Bottiglione F 2008 *J. Mech. Phys. Solids* **56** 2555
[12] Persson B N J 2007 *Phys. Rev. Lett.* **99** 125502
[13] Mindlin R D 1949 *J. Appl. Mech.* **71** 259
[14] Campañá C, Müser M H and Robbins M O 2008 *J. Phys.: Condens. Matter* **20** 354013
[15] See also Appendix A in Persson B N J *et al* 2008 *J. Phys.: Condens. Matter* **20** 395006
[16] Persson B N J 2008 *J. Phys.: Condens. Matter* **20** 312001
[17] Persson B N J, Bucher F and Chiaia B 2002 *Phys. Rev.* B **65** 184106
[18] Berthoud P and Baumberger T 1998 *Proc. R. Soc.* A **454** 1615
[19] Persson B N J 2006 *Surf. Sci. Rep.* **61** 201
[20] Hyun S, Pei L, Molinari J F and Robbins M O 2004 *Phys. Rev.* E **70** 026117
[21] Campañá C and Müser M H 2007 *Europhys. Lett.* **77** 38005
[22] Borri-Brunetto M, Chiaia B and Ciavarella M 2001 *Comput. Methods Appl. Mech. Eng.* **190** 6053
[23] Pei L, Hyun S, Molinari J F and Robbins M O 2005 *J. Mech. Phys. Solids* **53** 2385
[24] Persson B N J, Lorenz B and Volokitin A I 2010 *Eur. Phys. J.* E **31** 3
[25] Yang C and Persson B N J 2008 *J. Phys.: Condens. Matter* **20** 215214
[26] Yang C, Tartaglino U and Persson B N J 2006 *Eur. Phys. J.* E **19** 47
[27] Mo Y F, Turner K T and Szlufarska I 2009 *Nature* **457** 1116
[28] Lorenz B and Persson B N J 2009 *J. Phys.: Condens. Matter* **21** 015003
[29] Lorenz B, Carbone G and Schulze C 2010 *Wear* **268** 984
[30] Barber J R 2003 *Proc. R. Soc.* A **459** 53
[31] Campañá C and Müser M H 2006 *Phys. Rev.* B **74** 075420
[32] Yang C, Persson B N J, Israelachvili J and Rosenberg K 2008 *Europhys. Lett.* **84** 46004
[33] Yang C and Persson B N J 2008 *Phys. Rev. Lett.* **100** 024303
[34] Persson B N J 2002 *Eur. Phys. J.* E **8** 385
[35] Baltazar A, Rokhlin S I and Pecorari C 2002 *J. Mech. Phys. Solids* **50** 1397
[36] Nagy P G 1992 *J. Non-Destruct. Eval.* **11** 127 and references therein
[37] Akarapu S, Sharp T and Robbins M O 2010 arXiv:10.1479v1
Akarapu S, Sharp T and Robbins M O 2010 private communication